The 2010 IEEE/RSJ International Conference on
Intelligent Robots and Systems
October 18-22, 2010, Taipei, Taiwan

VSA-HD: From the Enumeration Analysis to the Prototypical Implementation

Manuel G. Catalano, Giorgio Grioli, Fabio Bonomo, Riccardo Schiavi and Antonio Bicchi

Abstract— **This paper presents design, implementation and performance of a new Variable Stiffness Actuator (VSA) based on Harmonic Drives (VSA-HD), which is an improvement over past work reported in [1], [2]. While previous prototypes have been developed to demonstrate the effectiveness of the variable stiffness actuation principle and the possibility to develop a compact and reliable actuator, the VSA-HD has been obtained by exploring the performance of the enumeration of all VSA made out a basic components set (i.e. two prime movers, two harmonic-drive gears, and the output shaft) and all the feasible interconnections between them as presented in [3]. Along this enumeration the VSA-HD conceptual layout has been selected as being good trade-off between mechanical complexity and overall performance.**

This paper discusses in depth the actuator mechanical layout, highlighting the main characteristics of the new design. A model for the actuator is introduced and validated by experimental results.

Index Terms— **Physical Human-Robot Interaction, Safety, Performance, Variable Stiffness Mechanisms, Actuators**

I. Introduction

Protecting human operators from unexpected impacts against robotic devices and physical Human-Robot Interaction (pHRI) have been the main motivations for the development of Variable Stiffness Actuators. The first generation of VSAs (e.g., [1] the first prototype our group proposed) was designed to demonstrate the effectiveness of the variable stiffness approach, not focusing on system performance and mechanical design.

Recently, the development of control techniques ([4], [5], [6], [7]) able to manage both stiffness and position at the output joint shaft has been opening new field of application such as energy efficiency for repetitive tasks (Uemura et al. [8]), or walking robots (Yamaguchi et al. [9]). VSAs shows also breaking strength in operations where the robot is interacting, or even colliding with the operator and/or the environment [10].

Many prototypes, often designed and optimized for a particular application, have been developed by the research community over the years. The VSJ presented by Choi et al. in [11] relies on the displacement control of two concentric permanent magnetic rings to implement stiffness variation, retrieving nearly zero minimum stiffness. The AMASC [12], designed for running/jumping robots and based on fiberglass springs serially connected to the main actuator, permits large energy storage, enabling high efficient walking thanks to the periodic transformation of kinetic energy to potential energy and vice versa. In [13] Wolf et al. present the VS-Joint, a variable stiffness joint for robotic arms, where the possibility to control the length of a set of springs acting on a cam profile allows the stiffness variation. The design of the cam profile, related to the stiffness-displacement characteristic, enable to adapt the actuator to different applications.

Authors are with Centro Interdipartimentale di Ricerca "'E. Piaggio"', University of Pisa, 56126 Pisa, Italy {r.schiavi}@centropiaggio.unipi.it

Fig. 1. VSA-HD final version of the prototype.

The VSA-HD has been designed by exploring the enumeration of all the possible variable stiffness actuators composed by a finite set of mechanical components (reference frame, output joint shaft, two prime mover, two harmonic drive gearboxes) and all the possible interconnection between them. The layout selection and the mechanical design were done pursuing the best trade-off between mechanical complexity and performance (stiffness, torque, and speed ranges at the output joint shaft).

This article is structured as follows: section II shortly reports the selection of the mechanical layout from the enumeration of all the possible actuators. Section III describes the conversion of the layout into a real mechanical solution, section IV illustrates the linear equivalent model of the actuator, while section V reports the experimental setup and the tests performed to validate the model and evaluate actuator performance. Finally, conclusions are drawn in section VI.

II. Layout Selection

The idea of selecting the mechanical design for a VSA through investigation of theoretical characteristics of the conceptual layout has been introduced in [3]. The basic idea

is to consider a VSA consisting of a basic set of *mechanical components* (i.e. prime movers, gearboxes, output shaft and mechanical frame), and a set of *mechanical connections* between them: rigid, elastic, or free. From the enumeration of all the possible arrangements, a preliminary performance analysis of the resulting actuator can be done. This study of conceptual layouts is limited to systems based on two prime movers, bidirectional non-linear elastic connections and Harmonic Drive (HD) gearboxes. The choice of HD systems is motivated by their small axial footprint, the nearly absent backlash, and the high ratio between reduction and weight/volume.

An HD comprises tree elements: the *Wave Generator* (WG) an elliptical disk with an outer bearing; the *Flex Spline* (FS) an externally pronged flexible element, internally connected with WG; and the *Circular Spline* (CS), a ring gear with slightly more teeth than FS. The behaviour of an HD is strictly related to the physical interconnection of these elements, for instance to implement a gearbox [14] WG is connected to the mover, CS to the frame, and finally FS to the output. In this configuration, when WG rotates, the teeth on FS get engaged with the corresponding on CS. For each revolution of WG the major axis of FS gets a displacement with respect to CS proportional on the difference of teeth between them. Another frequent use of HDs the implementation of a differential gearbox, one of the most useful configuration for the design of VSAs.

In [3], the application of the proposed methodology led to the isolation of 22 theoretical layouts of HD-based VSAs, differing for the topological configuration, and a further performance analysis of consented to group those designs into 5 equivalence classes or families. Each of those family includes a set of layouts with similar characteristics differing by number and topology of connections, thus showing different mechanical complexity.

For each layout it is possible to define a Performance Envelope (PE) in the space $\langle \tau, \omega, \sigma \rangle$, which is a three-dimensional extension of the traditional $\langle \tau, \omega \rangle$ motor charts. A schematization of the selection tree and the characteristic of the VSA-HD layout are shown in Fig.2, along with some performance indexes. The parameters considered along the selection are:

- Performance Envelope Volume (PEV) $\left[\text{Nm}\frac{\text{Nm}}{\text{rad}}\frac{\text{rad}}{\text{s}}\right]$: the volume of the actuator PE;
- Maximum Torque (τ_M) [Nm]: the maximum torque at the joint shaft;
- Maximum Stiffness (σ_M) [Nm/rad]: the stiffness reached for maximum motor activation:
- Maximum stiffness without external load ($\bar{\sigma}_M$) [Nm/rad];
- Stiffness Velocity ($\dot{\sigma}$) [Nm/s rad]: $\dot{\sigma} = \frac{\Delta\sigma}{T_\sigma}$ the ratio between the maximum stiffness variation and the time to achieve it, under maximum motor activation and negligible external disturbances.

The layout of VSA-HD has been selected from the e family, representing a good trade-off between mechanical

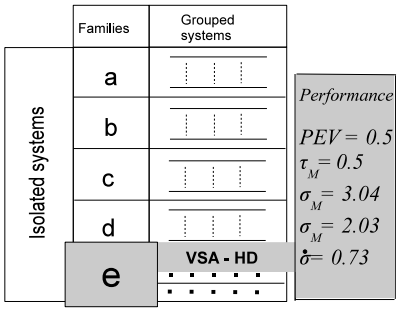

Fig. 2. Tree of the isolated layouts and relative families. In grey the selected layout and its performance. Data is extracted from the comparative analysis and normalized with respect to a system composed by an elastic connection between the motor and a fixed frame.

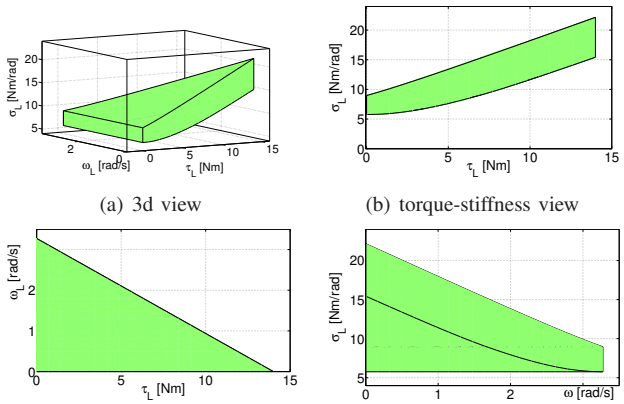

(a) 3d view (b) torque-stiffness view

(c) torque-speed view (d) speed-stiffness view

Fig. 3. Theoretical working volume of VSA-HD derived from the analisys performed in [3].

complexity and overall performance, and it is shown in Fig.5. Fig.3 shows the PE and its projections as derived in [3]. Results obtained in [3] are based on a generic non-linear elastic element with hyperbolic sine characteristic, VSA-HD uses an evolution of the four-bar mechanism as proposed in [2], thus presents the PE of Fig.4. The main differences

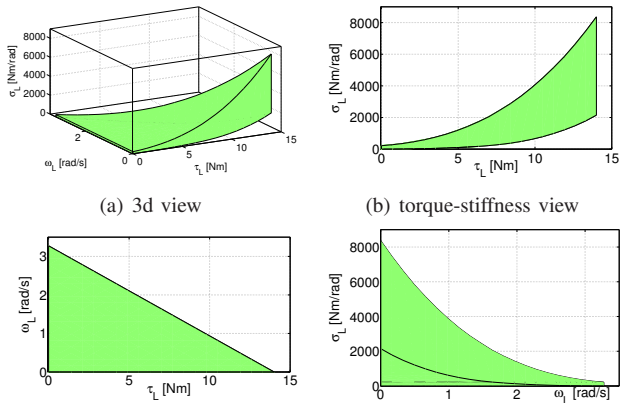

(a) 3d view (b) torque-stiffness view

(c) torque-speed view (d) speed-stiffness view

Fig. 4. The nominal working volume of VSA-HD, derived by performance of the motors and harmonic drives and through analitical solution of the non-linear spring characteristic. Differences from theoretical workspace of Fig.3 are due to the different assumptions about the non-linearity of the spring.

in the shape are due to the stronger non-linearity of the elastic elements.

III. Mechanical design

A. Mechanical layout implementation

The basic components constituting the VSA-HD are two Maxon brushless prime movers (EC305013 for q_1 and EC309756 for q_2) and two pancake Harmonic Drive gearboxes (HDUF-14-100, with a reduction ratio of 100:1). In these HDs a forth element called Dynamic Spline (DS) with the same number of teeth as FS replaces the traditional HD output. As in VSA-II (see [2]) four-bar linkages are adopted to implement the non-linear elastic elements. The final assembly of those basic components derives directly as the rendering of the selected theoretical layout in a mechanical solution. Fig.5 shows a schematic representation

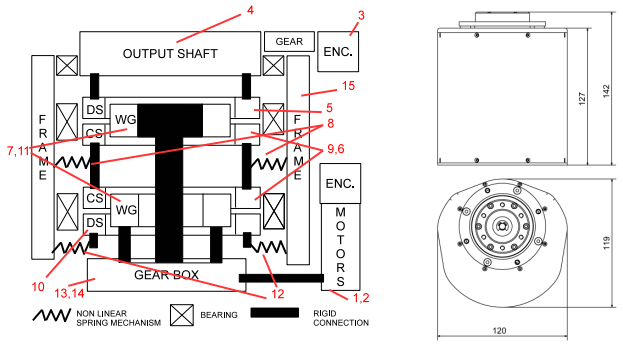

Fig. 5. Schematic representation of the real mechanical implementation (left); draft of the external appearance and dimension of VSA-HD (right)

of the real implementation (left) and a draft of the external appearance (right) with real dimensions.

Fig.6 shows a 3D section of the mechanical implementation. The prototype is essentially composed of a cylindrical rigid body (15) functioning as frame, where the HDs components are located and referred each other. The DS (10) presents an elastic connection to the frame through a pair of four-bar linkages (12). The two CSs (9,6) are fixed together and elastically connected to the frame through another pair of four-bar linkages (8). DS (5) is linked rigidly to the output shaft (4). The two WGs (7, 11) are actuated by the two motors (1, 2), placed outside the frame, the motion is transmitted by a double layer of linear gearboxes (13, 14). This first transmission layer implements a 1.6 : 1 speed reduction ratio. The output encoder (3) is connected to the output shaft with a linear gearbox. The main structure is enclosed by an external box (16).

This particular solution, based on a central main frame, is useful not only to guarantee mechanical tolerances and concentricity of HDs, but also to provide an output shaft capable of unlimited rotations around its axis. This solution gives the actuator the overall aspect of a traditional servo actuator, keeping at the same time a modular internal structure useful for scalability.

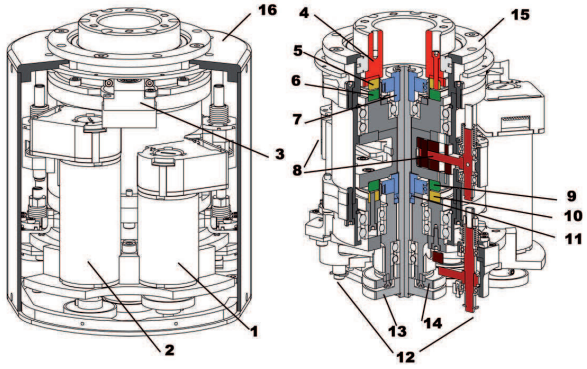

Fig. 6. Two 3D views of VSA-HD with basic components highlighted. Left panel shows a motor side view with a 3D section of the external box, while the right one shows a 3D section.

B. Variable Stiffness mechanism implementation

The four-bar mechanism, whose mathematical description is reported in Sec.IV, presents an intrinsic limitation due to a singularity: according to Fig.9,7 when the linkage L_1 trespass the position $q = 0$, cranks L_1, L_2, R_1 and R_2 are aligned, leaving the system evolution undetermined. To circumvent this problem a mechanical block could be used, preventing the system to reach the singularity, but at the cost of reducing the system PE. In the VSA-HD, instead, a cam profile is adopted to overcome the singularity. Fig.7 shows an isometric view of the lower part of the actuator with detail of the cam component: a sequence of screen-shots is reported to illustrate the singularity trespassing. The cam profile (red), centered in O, and its conjugate profile on link L_1 (green) are designed so as to guide L_1 when in proximity of its singular position. This solution preserves the PE allowing smaller value of minimum stiffness and giving the actuator pure symmetric bidirectional behaviour.

Actuator modularity and scalability is favoured by the possibility to interchange some components: L_1, R_1 and the torsional spring. Dimension and characteristics of adopted linkages and springs are reported in Sec.IV.

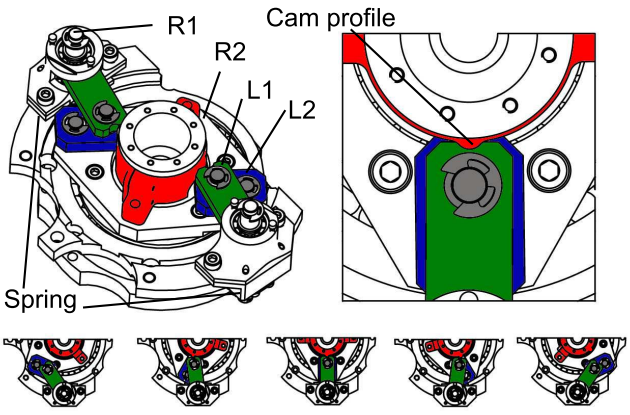

Fig. 7. Isometric view of the actuator lower side (left) with a couple of four bar linkages; detail of cam system (left) and screenshots sequence of linkages movements.

IV. MODEL

A. Non-linear Spring

The presence of a non-linear elastic transmission is a constraint on the design of a VSA. As previously explained the presented prototype relies on pairs of four-bar linkages. The behaviour of the mechanism, depicted in Fig.8, is described by the relationship between the angle q, the interface with the rest of the mechanical components, and angle β where the linear spring is mounted on (see Fig.9). Geometric considerations allow to explicit the relation as

$$\begin{aligned}\beta(q) &= \arccos\left(\frac{-R_1+R_2\cos(q)}{\sqrt{{R_1}^2+{R_2}^2-2R_1R_2\cos(q)}}\right)+ \\ &\quad -\arccos\left(\frac{L_1(R_1-R_2)-R_1R_2\,(1-\cos(q))}{L_1\sqrt{{R_1}^2+{R_2}^2-2R_1R_2\cos(q)}}\right)\end{aligned} \quad (1)$$

The potential energy stored in the spring $E(q) = k\beta^2(q)/2$ permits to express the torque $M(q)$ and the stiffness $\sigma(q)$, as

$$M(q) = \frac{\partial E(q)}{\partial q} = \frac{\partial E}{\partial \beta}\frac{\partial \beta}{\partial q}\,, \quad (2)$$

$$\sigma(q) = \frac{\partial^2 E(q)}{\partial q^2} = \frac{\partial E}{\partial \beta}\left(\frac{\partial^2 \beta}{\partial q^2}+\left(\frac{\partial \beta}{\partial q}\right)^2\right)\,. \quad (3)$$

B. Equilibria

To study the equilibria of the VSA-HD system we resort to the linear equivalent model of Fig.8. The system equilibrium conditions are described by the linear equation system

$$X_{W1}: \quad 0 = \tau_1 - R_1\sin(\alpha) \quad (4)$$

$$X_{W2}: \quad 0 = \tau_2 + R_5\sin(\alpha) \quad (5)$$

$$X_{FS1}: \quad 0 = \tau_L + R_1\sin(\alpha) - R_2\cos(\beta) \quad (6)$$

$$X_{FS2}: \quad 0 = R_3 - R_4\cos(\beta) \quad (7)$$

$$X_{CS1}: \quad 0 = \tau_{S1} + R_2\cos(\beta) - R_3 \quad (8)$$

$$X_{CS2}: \quad 0 = R_4\cos(\beta) - r_5\sin(\alpha) + \tau_{S2} \quad (9)$$

$$Y_{FS1}: \quad 0 = R_1\cos(\alpha) - R_2\sin(\beta) \quad (10)$$

$$Y_{FS2}: \quad 0 = R_5\cos(\alpha) - R_4\sin(\beta)\,, \quad (11)$$

where $\tau_{S1,S2}$ are the torques exerted by the two springs, $\tau_{1,2}$ produced by the motors (after the first gearbox), and τ_L is the load torque (refer to Fig.8 for other variables definition).

Solving the system, and substituting $\tan(\alpha)\tan(\beta) = 1/(N+1)$, it is possible to obtain the relationship between motors, springs, and link torques at the equilibria. This relationship can be made an explicit function of the spring torques

$$\tau_1 = \frac{1}{N+1}\tau_{S1} + \frac{1}{N+2}\tau_{S2} \quad (12)$$

$$\tau_2 = \frac{1}{N+2}\tau_{S2} \quad (13)$$

$$\tau_L = -\frac{N}{N+1}\tau_{S1} - \frac{N}{N+2}\tau_{S2}\,, \quad (14)$$

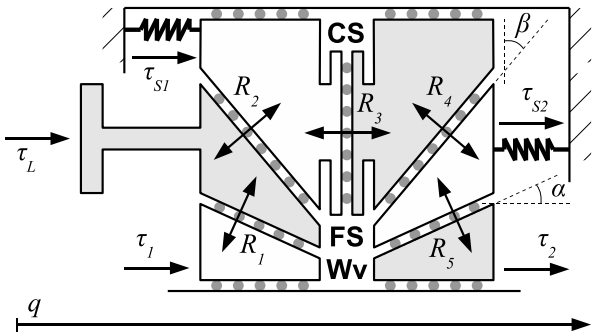

Fig. 8. Linear equivalent schematics of the VSA-HD system. Rotations of the bodies in the actuator are represented by translations in the x direction, and conversely forces are equivalent to Torques.

or, rearranging the previous equations, of the motor torques. The previous relationships can be slightly simplified under the working hypothesis of large N, thus $N+1 \approx N$.

Moreover, from the linear equation model of Fig.8 derives the mechanisms Willis formula, relating angular positions and speeds of all the moving components, obtaining

$$q_1 = (N+1)q_{FS1} - Nq_{CS1} \quad (15)$$

$$q_2 = (N+1)q_{FS2} - Nq_{CS2}\,. \quad (16)$$

A straightforward consequence of equation 14, is that with no load applied to the link, the equilibrium of the system is reached when the two springs are balancing. Considering equal and symmetric elastic elements implies the equality of their deformations $\bar{q}_s$ in opposed directions. The spring deformation angles q_{S1} and q_{S2} are defined as

$$q_{S1} = q_{CS1} \quad (17)$$

$$q_{S2} = q_{FS2}\,, \quad (18)$$

applying results of equations 15 and 16, the equilibrium position of the link as a function of the motor angles can be derived as follows. The spring balance $q_{CS1} = -q_{FS2}$ implies

$$q_{FS1} - N^{-1}q_1 = -N^{-1}q_2 - q_{CS2}\,,$$

remembering that $q_{CS1} = q_{CS2}$ (because of the rigid connection of the two CS elements), we have

$$q_{FS1} - N^{-1}q_1 = -N^{-1}q_2 - q_{CS1}\,.$$

Further application of equation 15 and 16, yields

$$q_{FS1} - N^{-1}q_1 = -N^{-1}q_2 - q_{FS1} + N^{-1}q_1\,,$$

which finally gets the relation

$$q_L = q_{FS1} = \frac{2q_1 - q_2}{2N} = \frac{1}{N}\left(q_1 - \frac{1}{2}q_2\right)\,. \quad (19)$$

From equations 15 and 16 it can be derived

$$\begin{aligned} q_{FS2} &= q_{CS1} = q_{FS1} + \frac{1}{N}q_1 \\ &= \frac{1}{N}\left(q_1 - \frac{1}{2}q_2\right) + \frac{1}{N}q_1 = -\frac{1}{2N}q_2\,. \end{aligned} \quad (20)$$

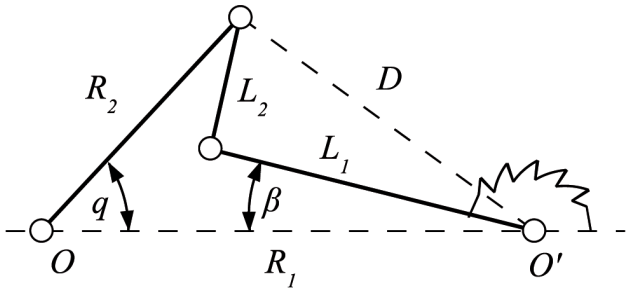

Fig. 9. Working principle of the non-linar spring used in the VSA-HD. Angle q is the interface between the non-linear elasticity and other system components. A linear spring is connected to the 4-bar linkages and excited by the angle β. The non-linearity comes from the variation in speed ratio between the cranks L_1 and R_2, ranging from a finite value to 0 (4-bars fully opened), thus giving rise to a stiffness ranging up to infinity.

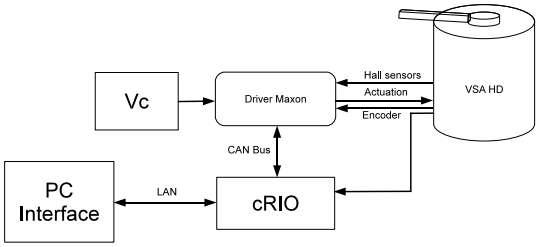

Fig. 10. Schematic of the experimental setup.

The last two equations 19,20 tell us that motor 1 is used to move the link and motor 2 is used to change the non-linear spring working point (and thus the stiffness). While motion of the output shaft does not need compensation of the stiffness angle, a change in the stiffness preset needs compensation by motor 1 to keep still the output equilibrium position. From equation 19 it holds

$$q_1 = \frac{1}{2} q_2 \,. \tag{21}$$

Finally, the composition of equations 3,14,17,18 enable to describe the output stiffness as

$$\sigma_L = \sigma_{S1} + \sigma_{S2} \,. \tag{22}$$

V. Experimental Results

A. Experimental Setup

Two Maxon brushless motors are driven by a pair of Maxon DES70/10 implementing low level torque control. An optical quadrature encoder (HEDS-5540) is used to detect the output joint shaft position. The main control loop is implemented by a CompactRIO (cRIO–9074) embedded controller by National Instruments. It implements CAN-bus communication with the motor drivers, detects the encoder signals, and receives commands/trajectories over an Ethernet link. Fig. 10 shows a schematic representation of the described setup. The control is performed by two nested loops: the cRIO implements the external one, while the motor drivers close the inner one. The external loop, running at 1 KHz, is responsible of the motor position control, implemented with a PID controller, acting on the reference torques which are fed to the drivers via CAN-bus.

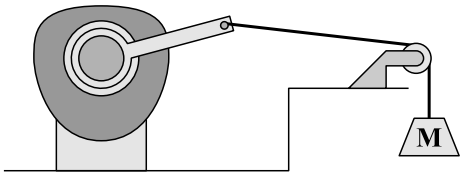

Fig. 11. Schematic of the Experimental setup for the Torque-Deformation evaluation. The link is an aluminium bar of length 200 mm. The text mass M used for the experiments was equal to 5 Kg.

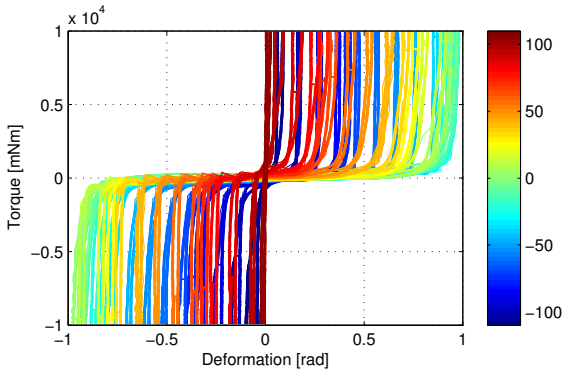

Fig. 12. Torque deformation chart. The line color is related to the position of the stiffness related angle q_2.

B. Torque-Stiffness characteristic

The controllable stiffness at the output shaft is generally related to the applied external torques. To evaluate the effective stiffness range several quasi-static experiments have been performed, measuring the deformation induced by an external load on the non-linear elasticity inside the actuator. The experimental setup is schematically illustrated in Fig. 11 while results are shown in Fig.12, for varying values of the controlled stiffness preset angle q_2. Several motion cycles have been performed for each q_2 value. The maximum and medium relative error measured on q_2 along all the experiments where smaller than 1% and 0.05% respectively. Interpolating the data collected during the cycles of each experiment a more accurate chart was extracted for comparison with the theoretical PE as illustrated in Fig. 13.

C. Stiffness Settling Time and Stiffness Velocity

Even though, many different parameters can be used to describe the performance of VSA systems, the time needed to set the desired stiffness is one of the most important. Several experiments have been performed to evaluate the parameter $\dot{\sigma}$ as defined in Sec.II.

To avoid undesired control effects, the time needed to reach the minimum stiffness from the maximum one has been measured by controlling the motors to their maximum activation level and switching to braking mode when the minimum value was reached. Fig. 14 shows the trajectories

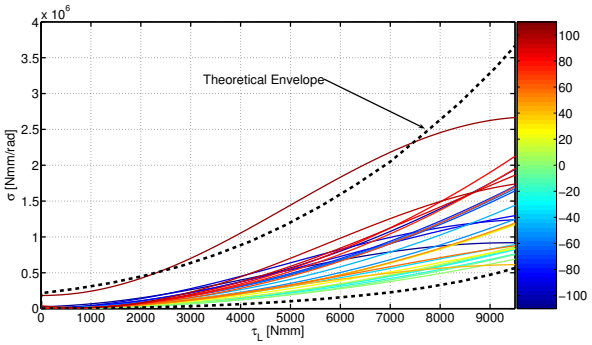

Fig. 13. Stiffness range as a function of the external load. Theoretical stiffness range (bold dashed line) and stiffness derived by data collected within experiments (colored lines). Experiments were performed in quasi-static condition, with $\omega_L \rightarrow 0$. The line color is related to the position of the stiffness related angle q_2.

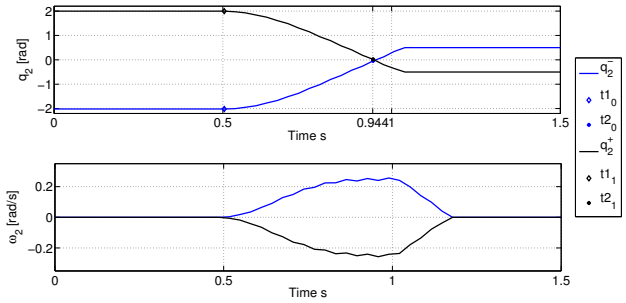

Fig. 14. Stiffness settling time: trajectories of q_2 during two experiments characterized by symmetric angles with maximum initial stiffness.

of q_2 during two of the recorded experiments, where the same maximum initial stiffness was obtained with two symmetric configurations. It can be noticed that the settling time, the time needed to switch from $\sigma_{\max}$ to $\sigma_{\min}$, and the trajectories of the stiffness related motor q_2 are not related to the initial configuration of the non-linear elastic transmission.

D. Performance

To fully characterize the performance of the VSA-HD the indexes defined in Sec. II have been evaluated and are reported in Table I.

τ_M	σ_M	$\bar{\sigma}_M$	$\dot{\sigma}$	ω
14	8000	200	450	3.2

TABLE I
EXPERIMENTAL PERFORMANCE PARAMETERS OF VSA-HD.

VI. CONCLUSIONS AND FUTURE WORK

In this paper a novel variable stiffness actuator prototype, namely VSA-HD, has been presented. The conceptual layout behind its design comes from a selection operated on the enumeration of all the possible VSAs based on the same set of mechanical components. After a detailed description of the mechanical implementation, a linear equivalent model is introduced to characterize the system behaviour and evaluate its theoretical performance. Finally, experimental results validating the effectiveness of the prototype and the theoretical results are reported.

Future work will include the exhaustive evaluation of performance parameters, improvement of the control algorithm and experimental validation of a 2 DOF variable stiffness arm based on VSA-HD.

VII. ACKNOWLEDGMENTS

Authors would like to acknowledge the useful work done by Andrea Gerace and Marco Lorenzetti. This work was partially supported by the VIACTORS Specific Targeted Research Projects, funded under 7th Framework Programme of the European Community under Contract IST-231554, and by the PRIN 2007 project SICURA, funded by the Italian Ministry of Education, University, and Research (MIUR). The authors are solely responsible for its content.

REFERENCES

[1] G. Tonietti, R. Schiavi, and A. Bicchi, "Design and control of a variable stiffness actuator for safe and fast physical human/robot interaction," in *ICRA 2005*. Barcelona, Spain: IEEE, April 18 – 22 2005, pp. 528 – 533.

[2] R. Schiavi, G. Grioli, S. Sen, and A. Bicchi, "VSA-II: A novel prototype of variable stiffness actuator for safe and performing robots interacting with humans," in *ICRA08*. Pasadena, CA, USA: IEEE, May 19 – 23 2008, pp. 2171 – 2176.

[3] M. G. Catalano, R. Schiavi, and A. Bicchi, "Mechanism design for variable stiffness actuation based on enumeration and analysis of performance," in *ICRA 2010*. Anchorage, Alaska: IEEE, May 3 – 8 2010.

[4] M. Uemura and S. Kawamura, "An energy saving control method of robot motions based on adaptive stiffness optimization - cases of multi-frequency components -," in *ICRA 2007*. Roma, Italy: IEEE, April 10 – 14 2007, pp. 551 –557.

[5] G. Palli, C. Melchiorri, and A. De Luca, "On the feedback linearization of robots with variable joint stiffness," in *ICRA 2008*, pp. 1753 – 1759.

[6] G. Palli and C. Melchiorri, "Robust control of robots with variable joint stiffness," pp. 1 – 6.

[7] A. D. Luca, F. Flacco, R. Schiavi, and A. Bicchi, "Nonlinear decoupled motion-stiffness control and collision detection/reaction for the vsa-ii variable stiffness device," in *IROS*. IEEE, 2009, pp. 5487–5494.

[8] M. Uemura and S. Kawamura, "Resonance-based motion control method for multi-joint robot through combining stiffness adaptation and iterative learning control," in *ICRA 2009*. Kobe, Japan: IEEE, May 12 – 17 2009, pp. 1543 –1548.

[9] J. Yamaguchi, D. Nishino, and A. Takanishi, "Realization of dynamic biped walking varying joint stiffness using antagonistic driven joints," in *ICRA98*. Leuven, Belgium: IEEE, May 16 – 20 1998, pp. 2002 – 2029.

[10] S. Haddadin, A. Albu-Schäffer, M. Strohmayr, M. Frommbergher, and G. Hirzinger, "Injury evaluation of human-robot impacts," in *ICRA08*, 2008, pp. 2203 – 2204.

[11] J. Choi, S. Park, W. Lee, and S.-C. Kang, "Design of a robot joint with vaiable stiffness," in *ICRA08*. Pasadena, CA, USA: IEEE, May 19 – 23 2008, pp. 1670–1765.

[12] J. Hurst, J. Chestnutt, and A. Rizzi, "An actuator with physically variable stiffness for highly dynamic legged locomotion," in *Proceedings of IEEE International Conference on Robotics & Aut.*, April 2004.

[13] S. Wolf and G. Hirzingher, "A new variable stiffness design: Maching requirements of the next robot generation," in *ICRA08*. Pasadena, CA, USA: IEEE, May 19 – 23 2008, pp. 1741 – 1746.

[14] T. D. Tuttle and D. Timothy, "Understanding and modeling the behavior of a harmonic drive gear transmission," Cambridge, MA, USA, Tech. Rep., 1992.

[15] *ICRA 2008, Proceedings of the 2008 IEEE International Conference on Robotics and Automation*. Pasadena, CA, USA: IEEE, May 19 – 23 2008.